SUPPLEMENTAL MATERIAL

Potent thrombolytic effect of N-Acetylcysteine on arterial thrombi.

Authors: Sara Martinez de Lizarrondo, PhD, Clément Gakuba, MD-PhD, Bradley A. Herbig, PhD, Yohann Repesse, PhD, Carine Ali, PhD, Cécile V. Denis, PhD, Peter J. Lenting, PhD, Emmanuel Touzé, MD-PhD, Scott L. Diamond, PhD, Denis Vivien, PhD, Maxime Gauberti, PhD.

Content:

Methods

Reagents

N-acetylcysteine, N-ethylmaleimide, collagenase type VII, aspirin, argatroban and ferric chloride ($FeCl_3$) were obtained from Sigma (Saint-Quentin-Fallavier, France). Mouse α-thrombin and human glu-plasminogen, fibronectin, plasminogen-free fibrinogen were obtained from Enzyme research laboratories (UK). The non-peptidic GpIIb/IIIa inhibitor GR144053 trihydrochloride came from Tocris and unfractioned heparin (UFH) was purchased from Sanofi-Aventis (France). Tissue-type plasminogen activator (tPA, Actilyse®) was obtained from Boehringer Ingelheim (Germany). Polyclonal anti-human VWF antibody and Seakemr HGT agarose used for *in vitro* VWF Multimer degradation studies came from Dako (Les Ulis, France) and Lonza (Walkersville, USA), respectively. Anti-α-CD41 (a platelet-specific marker) and anti-VWF used for immunofluorescence studies came from BD Biosciences and Fisher respectively. Sheep antiserum raised against fibrinogen/fibrin was prepared at the National institute for agronomic research (INRA, Clermont-Theix, France). Secondary F(ab')2 antibodies coupled to TRITC or FITC came from Jackson ImmunoResearch. Dotarem® came from Guerbet (Aulnay-sous-Bois, France).

Carotid artery thrombosis

Mice were placed on the back and a midline incision was performed in the neck. The right common carotid artery (CCA) was isolated. A piece of Whatman™ filter paper strip soaked in freshly prepared $FeCl_3$ (10%) was placed on the artery for 5 minutes and then removed. The blood flow was monitored using laser Doppler flowmetry in the territory of the right external carotid artery.

Magnetic resonance imaging (MRI) analyses

Experiments were carried out on a Pharmascan 7 T/12 cm system using surface coils (Bruker, Germany). T2-weighted images were acquired using a multi-slice multi-echo (MSME) sequence: TE/TR 51 /2500 ms with 70 × 70 × 500 μm^3 spatial resolution. Lesion sizes were quantified on T2 weighted images using ImageJ software (v1.45r). Magnetic resonance angiographies (MRA) were performed using a 2D-TOF sequence (TE/TR 10/50ms). Analyses of the MRA were performed blinded to the experimental data using the following score: 2: normal appearance, 1: partial occlusion and 0: complete occlusion of the MCA. For perfusion weighted imaging, a gradient echo fast imaging with steady state precession (GE-FISP) sequence was used with the following parameters: TR/TE 10 ms/5 ms (FA= 8°) with a temporal resolution of 911 ms and a spatial resolution of 100 × 100 × 75 μm^3 (half-scan). Mice were injected with 30 µL of a 0.5 M solution of Dotarem® (Guerbet, France) during repetitive image acquisitions. Then, ΔR2* images were generated using an in-house created macro in ImageJ. Perfusion index (ΔR2* peak ratios) was calculated by measurement of the ratio of ipsilateral and contralateral ΔR2*, as described previously[1].

Thrombus immunohistochemistry

Mice were perfused transcardially with heparinized-saline followed by a freshly prepared fixative solution (2% paraformaldehyde, 0.2% picric acid in phosphate buffer). Brains were cryoprotected (20% sucrose in veronal buffer, 24 h, 4°C) before cryostat sectioning. One set of horizontal brain sections (10 µm) was co-incubated with sheep anti-fibrinogen/fibrin (1:1000) and anti-α-CD41 (a platelet-specific marker, 1:1000; BD Biosciences) polyclonal antibodies. DAPI (Blue) was used to assess tissue morphology. When stated, brain sections were with both sheep anti-fibrinogen/fibrin (1:1000) and anti-VWF (1:600; Fisher) polyclonal antibodies. Secondary F(ab')2 coupled to TRITC or FITC (1:600; Jackson ImmunoResearch) were used for visualization under a microscope (Leica DM600). Images were digitally captured using a CoolSNAP™ camera and visualized with Metavue software (5.0).

VWF multimeric structure analysis and protein electrophoresis

The multimeric structure of VWF after NAC incubation was analyzed from human plasma by 0.1% SDS and 1.5% agarose (Seakemr HGT Agarose; Lonza Walkersville) gel electrophoresis as described before[2]. Pooled human plasma, purified fibrinogen, fibronectin, single-chain plasminogen (all from enzyme research laboratory) or recombinant single chain tPA (Actilyse) were separately incubated with NAC at 37°C for 1 hour, then the reaction was stopped by the addition of N-ethylmaleimide (Sigma) to alkylate the residual NAC, unless otherwise stated. VWF multimers were then examined by electrophoresis on a 1.5% SDS-agarose gel followed by immunoblotting using a horseradish-peroxidase-conjugated anti-human VWF polyclonal antibody. Other proteins were examined by electrophoresis on 3-8% NuPAGE Tris-acetate gels (Invitrogen) followed by Coomassie staining (Imperial Blue Staining, Thermo Scientifics).

Platelet aggregation/agglutination

Platelet aggregation and agglutination studies were performed on APAC4004 aggregometer (Elitech®, Sees, France). In both studies, increasing concentrations of NAC from 0 (saline) to 10 mM were added after the formation of platelet aggregates/agglutinates. Platelet aggregation was assessed in platelet rich plasma (PRP). Blood samples were collected and anti-coagulated with 3.8% tri-sodium citrate (9:1 v/v) and centrifuged for 10 minutes at 240g, at room temperature to produce PRP. Aggregation was initiated using 225 µl of PRP by addition of 25 µl Adenosine diphosphate (ADP, Helena Laboratories, UK; final concentration 5 µmol/l) or ristocetin (1.25 mg/ml, Stago®, Asnieres, France) with the platelet-poor plasma (PPP) 100% standard for change in optical density. GR-144053 (a GpIIb/IIIa inhibitor, analog to tirofiban, 50µg/mL) was added to the mixture when indicated. For platelet agglutination studies, human stabilized platelets (Von Willebrand Reagent, Siemens®) were resuspended in isotonic saline buffer containing 1mg/mL of ristocetin. Agglutination was induced using 200 µL of platelets

and 20 µL of normal human plasma. All experiments were recorded for 500 seconds and performed at least in triplicate.

VWF fibers formation under high shear rates

A 100 µm wide collagen strip was applied to a glass slide using a microfluidic patterning device as previously described[3]. A stenosis-shaped channel with a width of 15 µm was then placed perpendicularly on top of the collagen, so that collagen was only exposed in the constant-width region of the stenosis. Citrated platelet-free plasma (PFP) with or without NAC was then perfused through the device at 30,000 s-1 for 5 minutes, resulting in VWF fiber deposition on the collagen. After washing out the plasma with 0.5% BSA, labeling the VWF with fluorescent anti-VWF antibody, and then reducing the background with HBS, the now-fluorescent VWF fibers formed on the surface were able to be visualized. Once fluorescent images were captured of the VWF fibers, ImageJ was used to measure the length of and count each VWF fiber deposited in each channel.

Effect of NAC on fibrin-rich clot formation and dissolution *in vitro*

The effect of NAC during clot formation and lysis was studied by monitoring the change in turbidity in human plasma using a microplate reader (Fluostar Optima, BMG Labtech) as previously described[4]. Calcium Chloride (25 mmol/L final concentration) was added to citrated plasma diluted 1:2 in HEPES buffer (10 mM HEPES, 150 mM NaCl, and 0.4% BSA, pH=7.4) to promote coagulation. Samples were incubated at 37°C with NAC at different doses (0, 5, 10 and 20 mM) and absorbance (405nm) was monitored during 12 hours every 30 seconds at 37°C. When stated, tPA (0.5 nM) was also added to promote clot lysis. Results are expressed as the time to achieve 75% maximal absorbance (Clotting time, CT) and the rate of clot lysis was calculated as the time from initiation of clot formation to the time at which maximal absorbance falls to 50% (Clot Lysis time, CLT). All experiments were performed in triplicate.

Morphological studies of platelet agglutinates

Morphology and size of platelet agglutinates after NAC addition was assessed by bright-field microscopy. At the end of the monitoring of the agglutination studies, 5µL of the resulting platelet thrombi suspension in the NAC 0 mM (saline), 5mM and 10 mM conditions were obtained for image analyses. Laser-scanning confocal microscopy was performed using an inverted Leica SP5 confocal microscope (Leica Microsystems SAS) equipped with an Argon Gas laser and a X40 NA=1.4 oil immersion objective. Field of view was set at 1 µm x 1 µm with a 1024x1024 planar matrix (pixel size= 97.6 nm x 97.6 nm). Analyses were performed in triplicate and 10 images were randomly captured by sample.

Thromboelastography

For thromboelastography assays, fresh blood was drawn into 0.109 mol.L-1 trisodium citrate. Within 30 min, 300 µL of blood was added in INTEM® reagent vial (TEM®) in presence of increasing concentrations of NAC (0, 10 and 20 mM) with or without tPA (10 nM). Clotting time (CT), maximal clot firmness (MCF), the area under curve (AUC) and clot lysis time were measured to characterize and quantify the clot stability using rotational thromboelastography (ROTEM, TEM®).

Supplementary References

1. Pierce AR, Lo EH, Mandeville JB, Gonzalez RG, Rosen BR and Wolf GL. MRI measurements of water diffusion and cerebral perfusion: their relationship in a rat model of focal cerebral ischemia. *J Cereb Blood Flow Metab*. 1997;17:183-90.
2. Adam F, Casari C, Prevost N, Kauskot A, Loubiere C, Legendre P, Reperant C, Baruch D, Rosa JP, Bryckaert M, de Groot PG, Christophe OD, Lenting PJ and Denis CV. A genetically-engineered von Willebrand disease type 2B mouse model displays defects in hemostasis and inflammation. *Sci Rep*. 2016;6:26306.
3. Colace TV and Diamond SL. Direct observation of von Willebrand factor elongation and fiber formation on collagen during acute whole blood exposure to pathological flow. *Arterioscler Thromb Vasc Biol*. 2013;33:105-13.
4. Marcos-Contreras OA, Martinez de Lizarrondo S, Bardou I, Orset C, Pruvost M, Anfray A, Frigout Y, Hommet Y, Lebouvier L, Montaner J, Vivien D and Gauberti M. Hyperfibrinolysis increases blood-brain barrier permeability by a plasmin- and bradykinin-dependent mechanism. *Blood*. 2016;128:2423-2434.

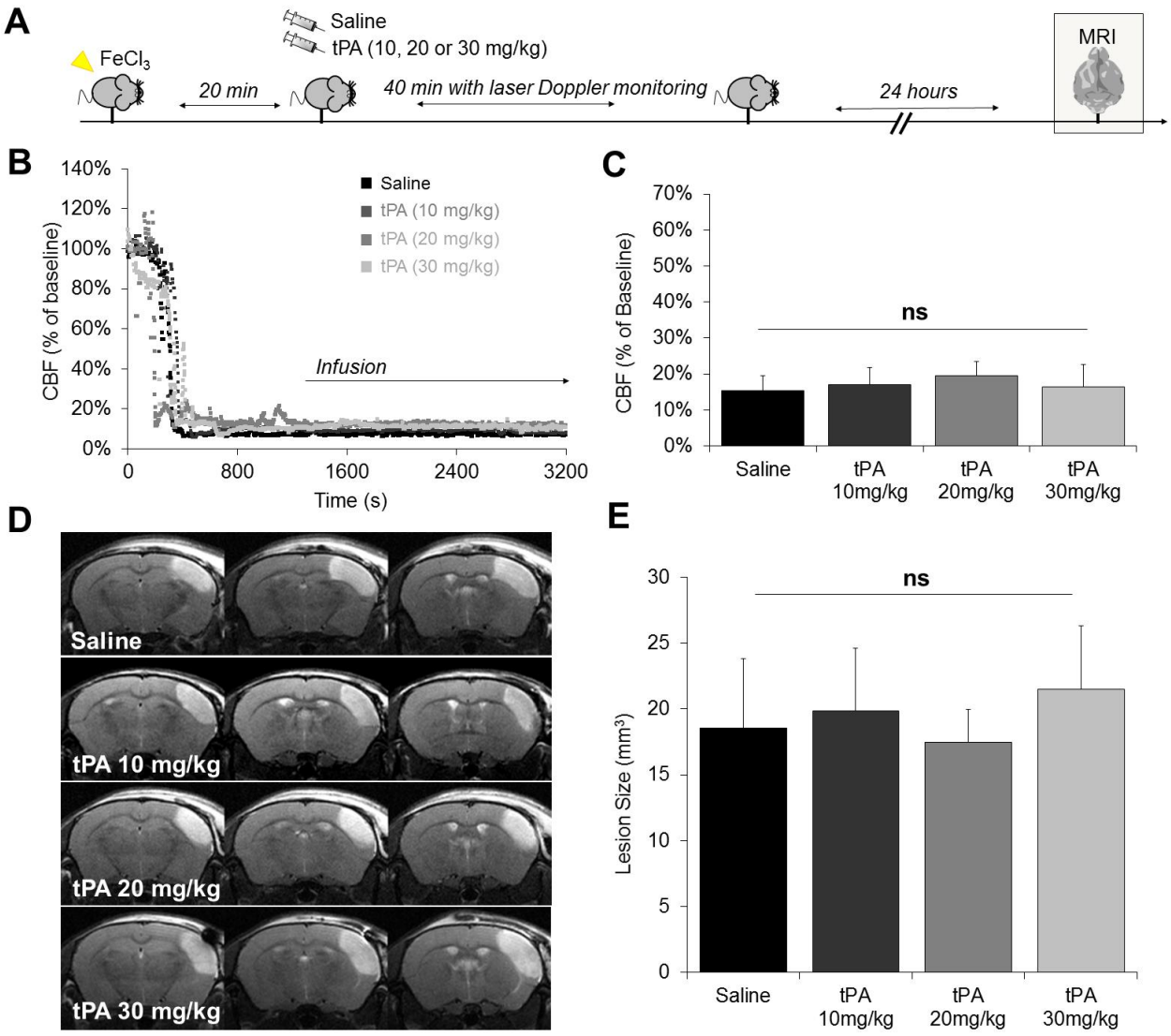

Figure S1: Thrombi in the $FeCl_3$ model are resistant to a wide range of tPA doses. (A) Schematic representation of the performed experiments. (B) Representative laser Doppler profiles of mice treated with an intravenous infusion of saline or tPA (10, 20 or 30 mg/kg) 20 min after MCAo. (C) Mean cerebral blood flow (CBF) (assessed by laser Doppler flowmetry 60 min after MCAo) of mice treated with saline or tPA 20 min after MCAo. (D) Representative consecutive slices of T2-weighted images of saline and tPA-treated (10, 20 or 30 mg/kg) mice 24 hours after $FeCl_3$ application. (E) Corresponding mean ischemic lesion sizes at 24 hours post-MCAo. (n=5-6 per group).

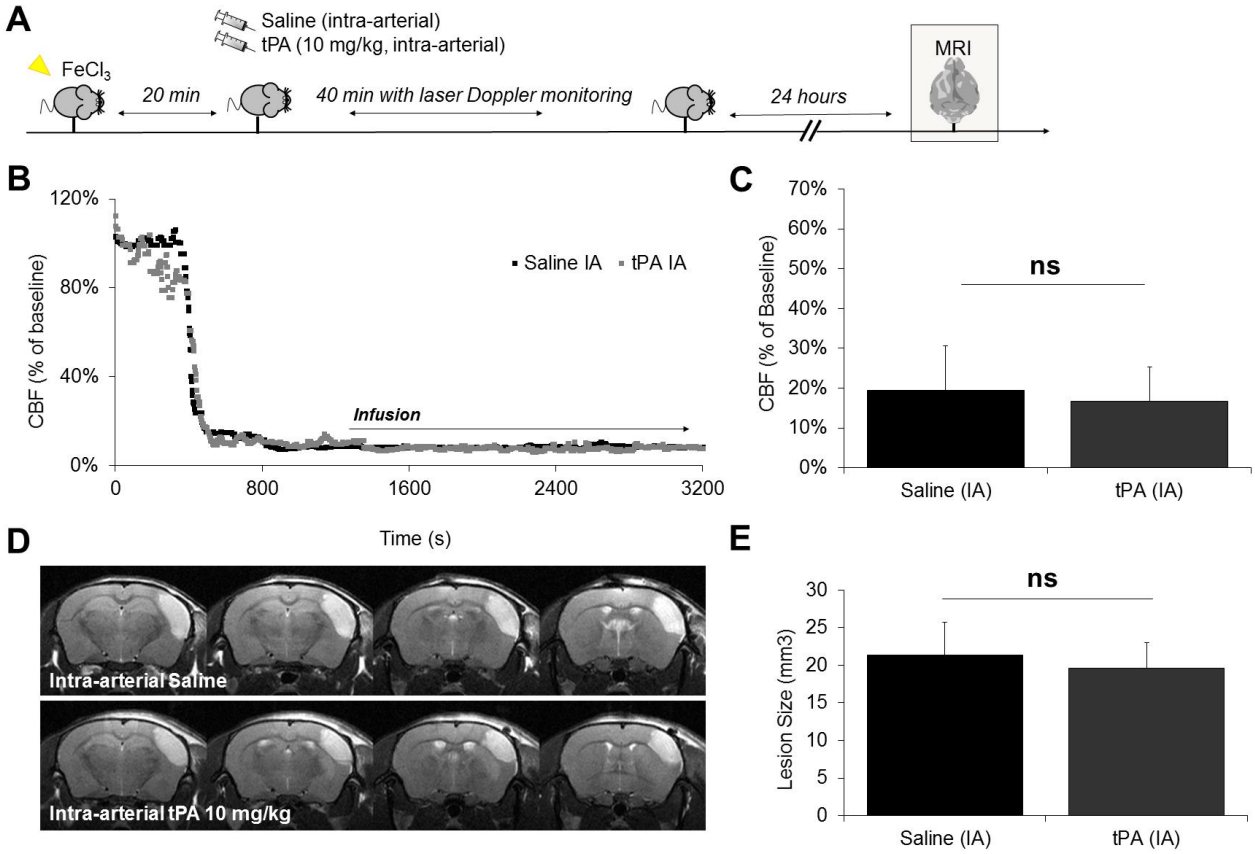

Figure S2: Thrombi in the $FeCl_3$ model are resistant to intra-arterial tPA administration. (A) Schematic representation of the performed experiments. (B) Representative laser Doppler profiles of mice treated with an intra-arterial infusion of saline or tPA (10 mg/kg) 20 min after MCAo. (C) Mean cerebral blood flow (CBF) (assessed by laser Doppler flowmetry 60 min after MCAo) of mice treated with intra- arterial saline or tPA 20 min after MCAo. (D) Representative T2-weighted images of intra- arterial saline and tPA-treated (10 mg/kg) mice 24 hours after FeCl3 application. (E) Corresponding mean ischemic lesion sizes at 24 hours post-MCAo. (n=4 per group). IA= Intra-arterial.

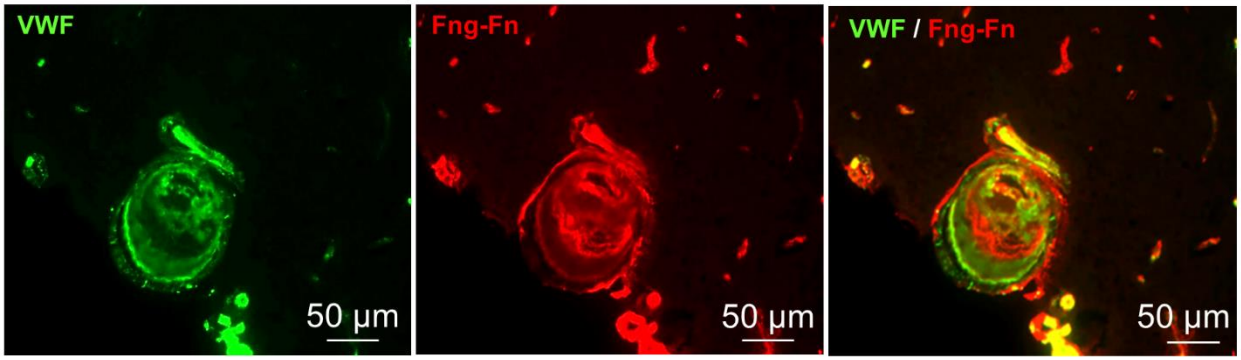

Figure S3: Thrombi in the thrombin model are rich in VWF and Fibrinogen-Fibrin. Representative immunohistological staining for VWF and fibrinogen-fibrin (Fg-Fn) of the MCA 20 minutes after thrombin-induced thrombosis.

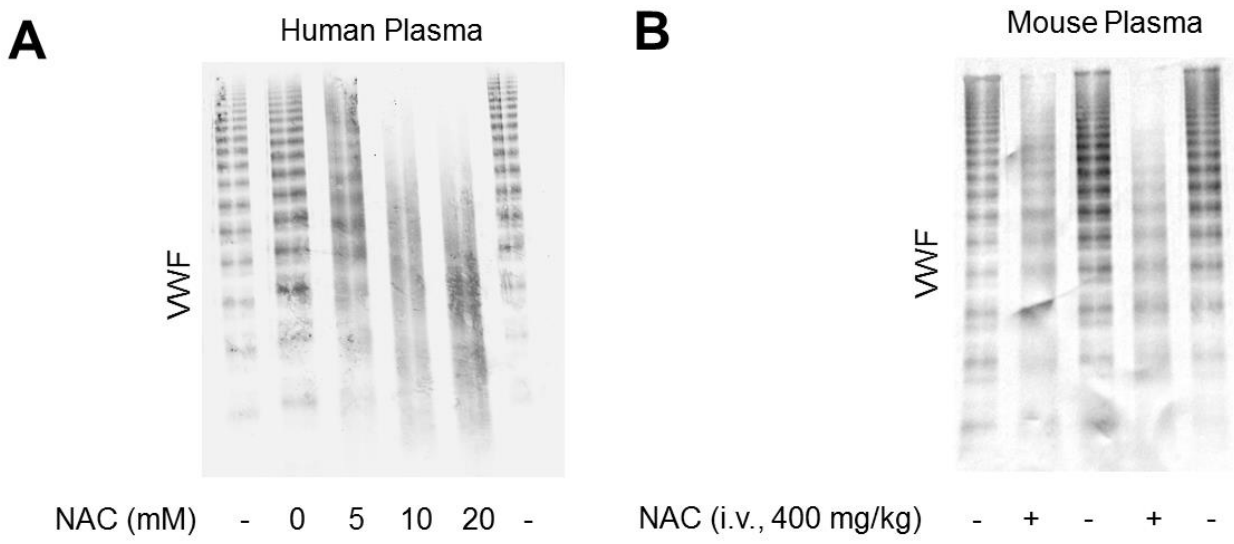

Figure S4: NAC reduces VWF multimers *in vitro* and *in vivo*. (A) Pooled human plasma was incubated with NAC at 37°C for 1 hour, then the reaction was stopped by the addition of N-ethylmaleimide to alkylate the residual NAC (except in the control '-' labeled lanes). VWF multimers were then examined by electrophoresis on an SDS-1.5% agarose gel followed by immunoblotting. NAC reduced VWF multimer size in a concentration-dependent manner *in vitro*. (B) Mice received a single intravenous injection of NAC (400 mg/kg) or an equivalent volume of saline. Blood samples were harvested 1 hour after injection. VWF multimers were then examined by electrophoresis on an SDS-1.5% agarose gel followed by immunoblotting (representative of n=5/group). NAC reduced circulating VWF multimer size *in vivo.*

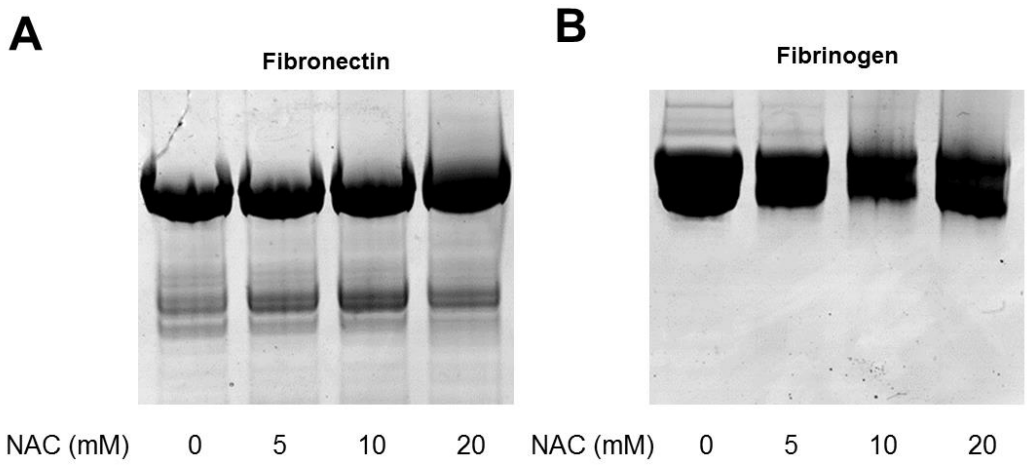

Figure S5: NAC has no significant effect on the molecular weight of fibronectin and fibrinogen. Purified human fibronectin (A) and human fibrinogen (B) were incubated with NAC at 37°C for 1 hour, then the reaction was stopped by the addition of N-ethylmaleimide to alkylate the residual NAC. Then, fibronectin and fibrinogen were examined by electrophoresis on 3-8% NuPAGE Tris-acetate gels followed by Imperial protein staining (Coomassie).

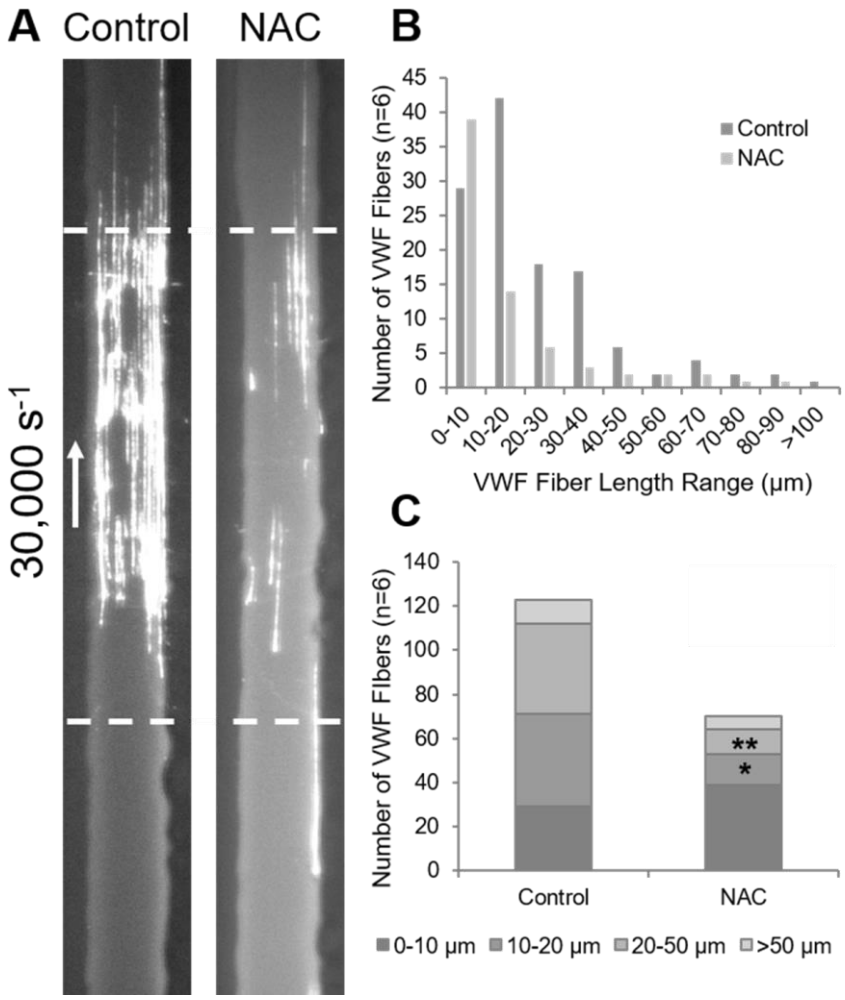

Figure S6: NAC reduces VWF aggregation on collagen. (A) Citrated platelet free plasma with either NAC (30 mM) or Hepes buffered saline (HBS) (control) was perfused over a 100 µm wide collagen strip at 30,000 s^{-1} for 5 min. The channel was then washed with 0.5% BSA, labeled with a polyclonal fluorescent anti-VWF antibody in HBS, and then HBS to reduce background before imaging. (B) The length of each VWF fiber in each image was measured, resulting in a size distribution of VWF fibers for both the control and NAC conditions. (C) Addition of NAC in citrated plasma resulted in a lower number of VWF fibers formed, and a significantly reduced number of 10-20 µm and 20-50 µm fibers compared to the control. (* means $p<0.05$; ** means $p<0.01$).

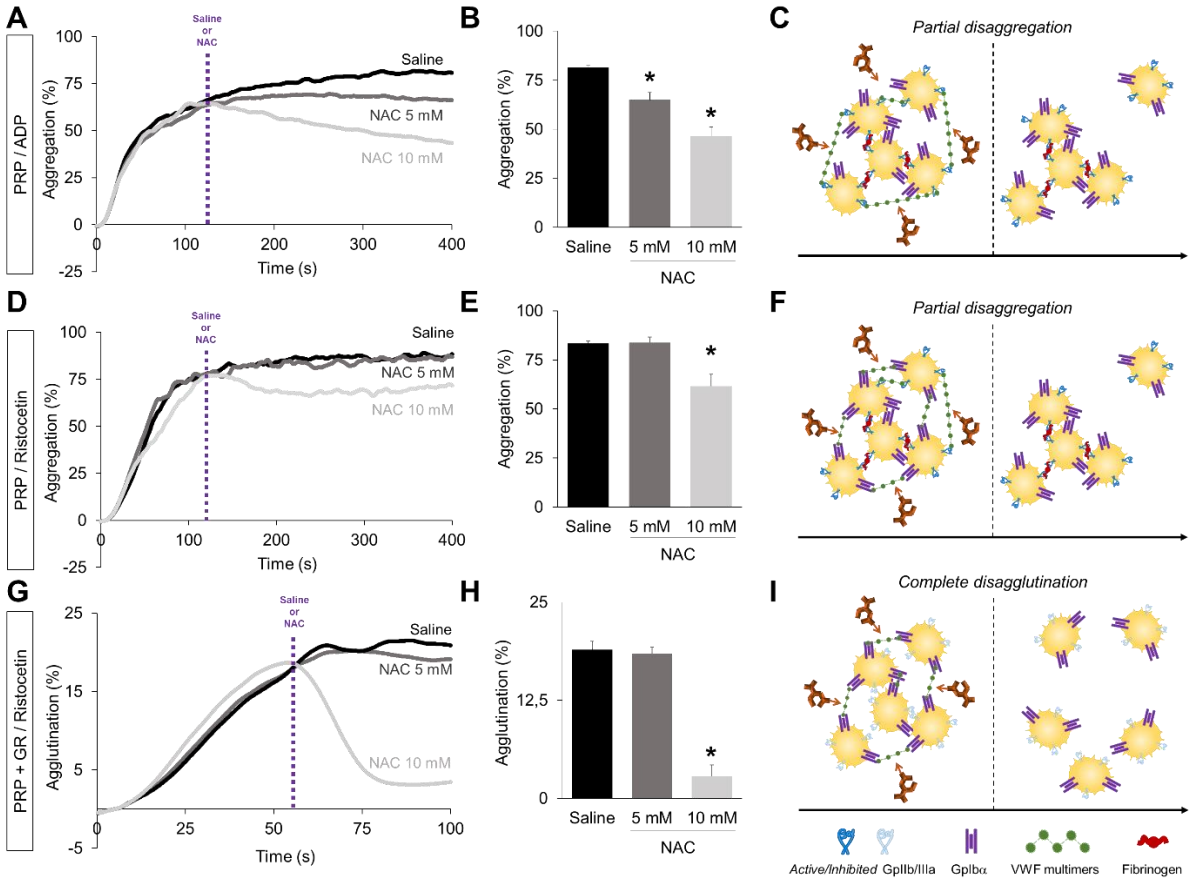

Figure S7: NAC has a direct effect on the stability of human platelet aggregates after ADP or ristocetin-induced aggregation. (A) Representative aggregation and disaggregation curves of platelets from platelet-rich plasma (PRP) in the presence of ADP before and after either saline or NAC treatment (0, 5 or 10 mM). (B) Corresponding quantification (n=3/group) at the end of the monitoring period. (C) Schematic representation of the effect of NAC after ADP-induced platelet aggregation. (D) Representative aggregation and disaggregation curves of platelets from platelet-rich plasma (PRP) in the presence of ristocetin before and after either saline or NAC treatment (0, 5 or 10 mM). (E) Corresponding quantification (n=3/group) at the end of the monitoring period. (F) Schematic representation of the effect of NAC after ristocetin-induced platelet aggregation. (G) Representative aggregation and disaggregation curves of platelets from platelet-rich plasma (PRP) in the presence of ristocetin and a GpIIb/IIIa inhibitor (GR144053, GR, 50 µg/ml) before and after either saline or NAC treatment (0, 5 or 10 mM). (H) Corresponding quantification (n=3/group) at the end of the monitoring period which was shortened to account for the instability of the platelet aggregates in this condition (spontaneous disaggregation). (I) Schematic representation of the effect of NAC after ristocetin-induced platelet aggregation in the presence of a GpII/IIIa antagonist. (* means significant versus saline).

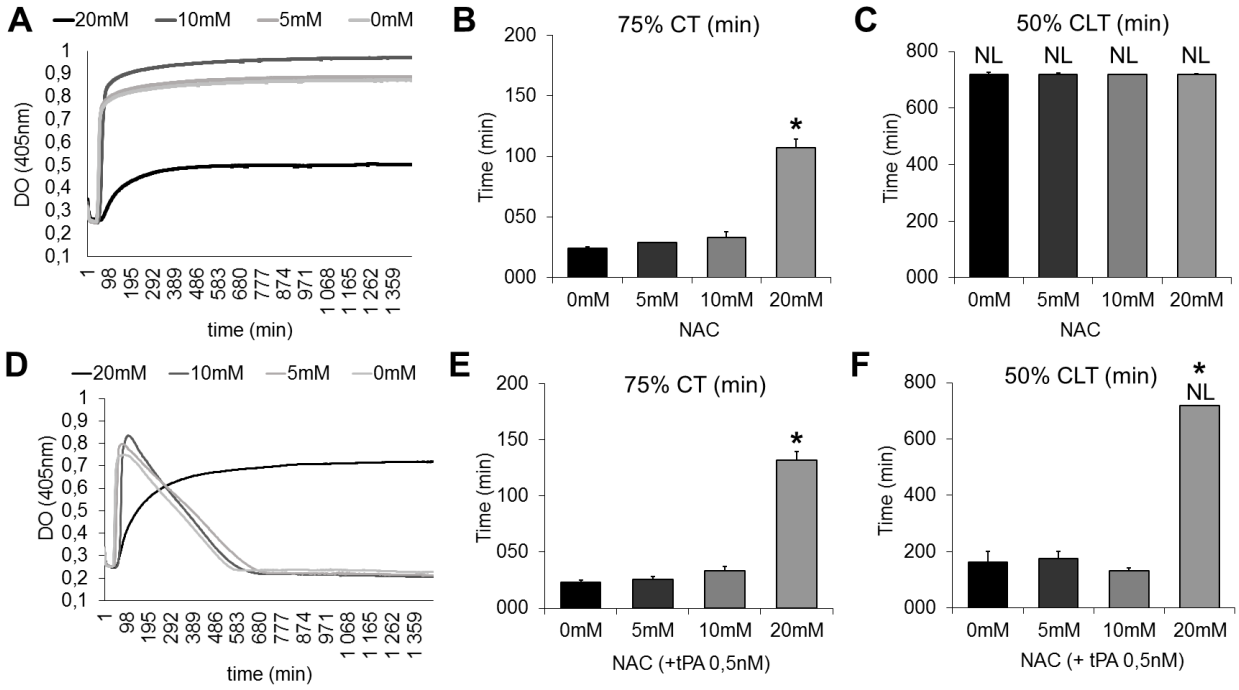

Fig. S8: Impact of NAC on coagulation and tPA-mediated fibrinolysis in vitro. (A) Kinetics of clot formation/lysis at different concentrations of NAC (0, 5, 10 and 20mM) in a turbidimetric assay in human plasma in absence of tPA. (B) Quantitative analysis of 75% of clotting time (75% CT), revealing that only the higher dose of NAC at 20mM significantly delays coagulation, without significant effects at lower concentrations. (C) Quantitative analysis of 50% clot lysis time (50%CLT), revealing that in the absence of tPA, NAC does not promote/affect endogenous fibrinolysis. (D) Kinetics of clot formation/lysis at different concentrations of NAC (0, 5, 10 and 20mM) in a turbidimetric assay in human plasma in presence of 0.5nM of tPA. (E) Quantitative analysis of 75% CT, revealing that only the higher dose of NAC at 20mM significantly delays coagulation in the presence of tPA. (F) Quantitative analysis of 50% CLT, revealing that NAC affects tPA-mediated fibrinolysis only at the highest studied concentration (20 mM), without significant effects at lower concentrations. All experiments were performed in triplicate and independently replicated 3 times (n=3). (* means significant versus 0mM condition). NL= no lysis observed. CT= Clotting time. CLT= Clot lysis time.

A

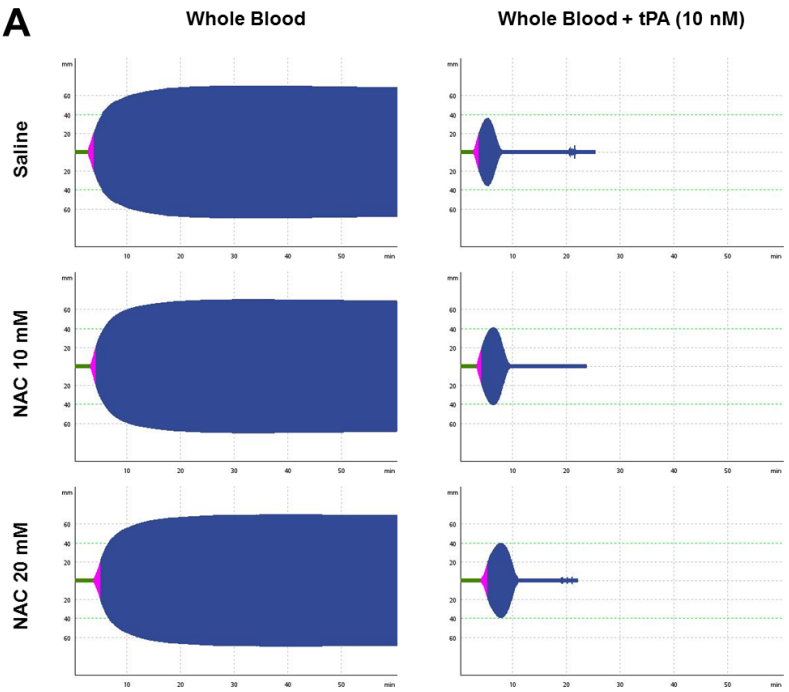

B

	Clotting Time (s)	Maximal Clot Firmness (mm)	Area Under Curve (mm.min)	ΔLysis Time (s)
Saline	154	70	6 958	---
NAC 10 mM	180	70	6 996	---
NAC 20 mM	216	69	7 073	---
tPA	152	36	3 569	301
NAC 10 mM tPA	185	40	4 025	304
NAC 20 mM tPA	233	40	4 496	406

Figure S9: Dose-dependent effects of NAC on ROTEM parameters using human whole blood. (A) Representative ROTEM profiles of human whole blood incubated with different concentrations of NAC (saline, 10 mM and 20 mM) with or without 10 nM tPA. (B) Corresponding quantifications showing mild prolongation of clotting time and reduced area under curve in the presence of 10 mM and 20 mM NAC. Only the highest concentration (20 mM) impacted the lysis time in line with our euglobulin lysis time results.

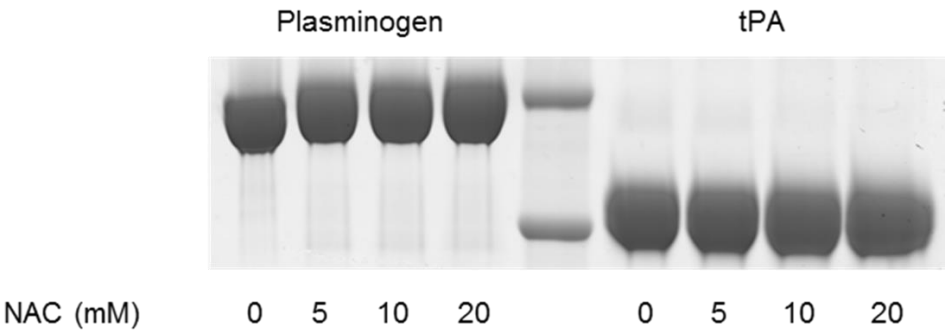

Figure S10: NAC has no significant effect on the molecular weight of plasminogen and tPA. Purified human plasminogen and recombinant human tPA were incubated with NAC at 37°C for 1 hour, then the reaction was stopped by the addition of N-ethylmaleimide to alkylate the residual NAC. Then, plasminogen and tPA were examined by electrophoresis on 3-8% NuPAGE Tris-acetate gels followed by Imperial protein staining (Coomassie).

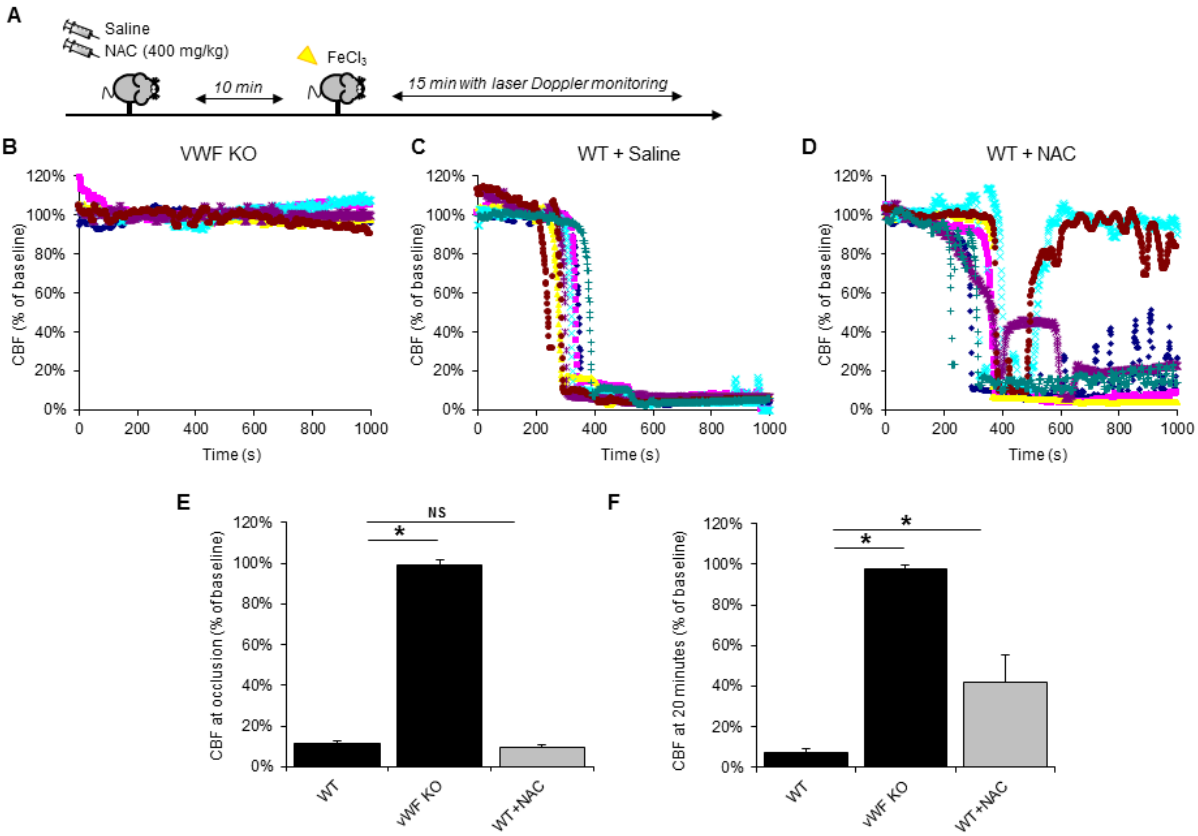

Fig. S11: CBF in the $FeCl_3$ model in VWF knock-out (KO) mice and wild-type (WT) NAC pre-treated mice. (A) Schematic representation of the performed experiments. (B) Representative Doppler flowmetry after $FeCl_3$ injury on the MCA (monitoring during 15 min) of saline-pretreated VWF KO (B) mice, saline-pretreated WT mice (C), and NAC-pretreated (400 mg/kg) WT mice (D). (E) Mean occlusion time. (F) Mean CBF at the end of the monitoring period.